


Real-Time Visualization of Internal and External Concentration Fields in Multiphase Systems via Laser-induced Fluorescence and Rainbow Schlieren Deflectometry During and After Droplet Production

Jens Stefan Heine^{1,‡,*}, Joschka Marco Schulz^{2,‡,*}, Henning Junne², Lutz Böhm², Matthias Kraume², and Hans-Jörg Bart^{1,*}

DOI: 10.1002/cite.202000135

 This is an open access article under the terms of the Creative Commons Attribution License, which permits use, distribution and reproduction in any medium, provided the original work is properly cited.

Dedicated to Prof. Dr.-Ing. Matthias Kraume on the occasion of his 65th birthday

The applicability of laser-induced dye fluorescence (LIF) and rainbow schlieren deflectometry (RSD) for qualitative, non-invasive real-time visualization of spatial concentration distributions in two standard reference systems is presented. The combination of LIF and RSD enables measurements inside and outside of droplets and is able to overcome limitations of both measurement techniques. Experimental results in the presence of interfacial phenomena are compared and the connection between inner and outer effects is shown during droplet production at a capillary.

Keywords: Concentration field, Laser-induced fluorescence, Marangoni convection, Mass transfer, Rainbow schlieren deflectometry, Real-time visualization

Received: July 10, 2020; *revised:* September 22, 2020; *accepted:* November 10, 2020

1 Introduction

In many industrial processes, e.g., in chemical engineering, temperature and concentration gradients significantly affect the mass- and heat transfer rates. However, the fundamentals are still not fully understood. In that respect, the understanding of mass transfer near the interface of liquid-liquid systems with interfacial instabilities, such as Marangoni convection [1], is very important for the efficiency of liquid-liquid contactors. The Marangoni effect leads to a strong coupling between concentration and velocity field, and therefore, significantly influences the mass transfer rate. The smallest unit in liquid-liquid systems constitutes the single droplet. During a droplet life three stages can be identified: (I) droplet formation with droplet detachment and acceleration, (II) droplet sedimentation, and (III) droplet coalescence [2]. Each of these stages has an effect on droplet mass transfer and should be analyzed separately [3, 4]. Complex physical phenomena on the single droplet scale include deformation of the interface, Marangoni effects and oscillations resulting in nonlinear mass transfer [5]. In many cases, interfacial phenomena dominate large-scale properties such as mass transfer rates or hold-up. To analyze complex processes at the interface in a detailed way,

it is necessary to simplify the system by implementing a stationary environment around a single droplet. This enables accurate determination of the mass transfer behavior at a given surface area. Concentration and interfacial tension as well as shear distribution along the interface causing Marangoni instabilities can thus be analyzed [5–9]. However, the mass transfer behavior is concentration dependent, whereby three different mass transfer regimes may exist starting from high to low concentration gradients [10]. The first two occur in case of high gradients and eddy diffusion and the third one is dominated by molecular diffusion [11]. To achieve a detailed analysis, optical measurement tech-

¹Jens Stefan Heine, Prof. Dr. Hans-Jörg Bart
jens.heine@mv.uni-kl.de, bart@mv.uni-kl.de
Technische Universität Kaiserslautern, Thermische Verfahrenstechnik, Gottlieb-Daimler Straße, 67663 Kaiserslautern, Germany.

²Joschka Marco Schulz, Henning Junne, Lutz Böhm,
Prof. Dr.-Ing. Matthias Kraume
j.schulz@tu-berlin.de
Technische Universität Berlin, Chair of Chemical and Process Engineering, Ackerstraße 76, 13355 Berlin, Germany.

[‡]These authors contributed equally to this work.

niques in general have the advantage of being less invasive, flexible, and offering high spatial and/or temporal resolutions [12] compared to conventional mass transfer measurements where samples have to be collected.

As every measuring technique has its respective shortcomings (see, e.g., Hohl et al. [9] for an overview regarding experimental applications in multiphase systems), the combination of LIF and RSD may overcome the limitations of both experimental techniques and therefore improve the experimental insight into disperse liquid-liquid systems on a single drop basis. LIF is theoretically capable of measuring dye concentrations inside and outside of a droplet simultaneously, the partitioning of the dye limits the simultaneous accessibility of the internal and external concentration field as shown exemplarily in Fig. 1 for the mass transfer of acetone from a toluene drop into stagnant water as continuous phase. As can be seen, the visualization of the external concentration field (Fig. 1b) by application of Rhodamin 6G is not suitable due to an overlighting effect of the inside of the drop: The hydrophobic nature of the dye necessitates larger laser power for the visualization in the surrounding water, which in turn leads to the overexposure inside the drop. To circumvent this problem RSD is used for visualization of the concentration distribution outside of the droplet (as shown exemplarily in [9, 23]), while LIF measurements are used inside the droplet [5, 6].

The measuring principle of RSD is based on deflection of collimated light rays due to presence of density inhomogeneities. By application of color scale filters density gradients are color coded and therefore made visible [13]. Since RSD is based on deflection of collimated light rays a measurement inside of the droplet is not possible due to the curvature of the surface of the drop, which leads to a strong displacement in the filter plane and therefore no color-coded information can be measured inside of the drop as shown in Fig. 1c. Taking a close look at the Schlieren image, light passing through the center of the drop can be detected as a result of only small deviations from perpendicular orientation between the collimated light rays and the surface area in the center region.

In case of symmetric conditions a quantitative evaluation is possible [14]. Since the concentration field is strongly inhomogeneous, instationary and most-likely asymmetric in the presence of interfacial effects, RSD is used for qualitative visualiza-

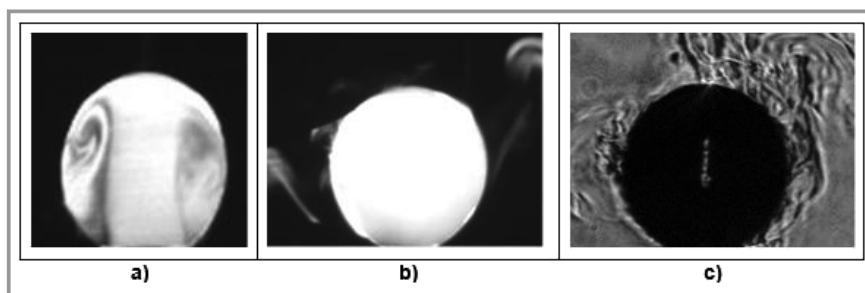


Figure 1. Visualization of mass transfer of acetone in toluene/water by LIF: intensity (laser power) tuned for measurement a) inside and b) outside of the drop, c) RSD measurement for the same system.

tion purposes. Nevertheless, the comparison with LIF gives a deeper insight into the occurring mass transfer phenomena and is able to explain the mass transfer behavior measured by conventional suction experiments.

Schlieren imaging was used for visualization of different phenomena in the past, see, e.g. Settles [15] for an extensive overview of past applications and Settles and Hargather [16] for a review of recent developments due to technical advances in digital photography and illumination technology. While qualitative optical investigations in liquid-liquid systems are summarized in Sawistowski [17], more recent results for the visualization of the Marangoni effect via Schlieren Deflectometry can be found elsewhere [18–20].

Tab. 1 summarizes the main characteristic of both measuring techniques. It is worthy to note that the spatiotemporal resolution for both techniques depends on the applied camera and lens system in combination with the intensity of the light source [9]. The given values are the ones realized during the experiments shown in this publication but may be improved to yield even higher resolutions. The measurement of concentration inside or outside a pendant drop is also possible by other measuring methods, such as Raman spectroscopy [5, 21]. Though the advantage of a direct measurement of the transfer component is given there, usually neither the temporal resolution nor the full-field nature are comparable to LIF or RSD [9].

Table 1. Comparison of characteristics of both measurement techniques.

Trait	LIF	RSD
Measuring domain	2D cut/sheet	2D/3D integral/volume
Temporal resolution [fps]	> 800	40–120
Distinction between several components	no	no
Invasivity	quasi non-invasive	non-invasive
Direct measurement	no	no
Visualized property	dye concentration field attached to solute	concentration gradient field of solute

2 Materials and Methods

Experiments are performed in two experimental setups located at the Chair of Separation Science and Technology at TU Kaiserslautern (TUK) and at the Chair of Chemical and Process Engineering at TU Berlin (TUB). LIF measurements were conducted at TUK, RSD measurements at TUB and suction experiments at both institutes.

2.1 Laser-induced Fluorescence at TUK

The test cell (1) shown in Fig. 2 [5] was made of glass, PTFE, and stainless steel, and is equipped with a heating/cooling jacket using a Thermo Haake K10/DC30 thermostat at an operating temperature of 25 °C. The droplet size control (2) on a stainless steel capillary ($d_i = 0.8$ mm, $d_o = 1$ mm) is done via high precision syringe pump (8) (Hamilton PSD/3 mini). The laser beam (gem 532, Laser Quantum) (6) passes through the ultra-fast motorized laser beam shutter (standa) (5), which is triggered by the high-speed camera (IDT Os8) and subsequently widened to a flat beam by lenses (4) and directed into the measurement cell (1). The image series (224 × 256 px) in this work were taken with 800 fps, meaning that the ultra-fast motorized laser beam shutter opened 800 times per second (up to 1000 openings are possible). Therefore, the laser with a wavelength of 532 nm and 1000 mW (possible are 50 mW up to 2000 mW) always has the same intensity for each image

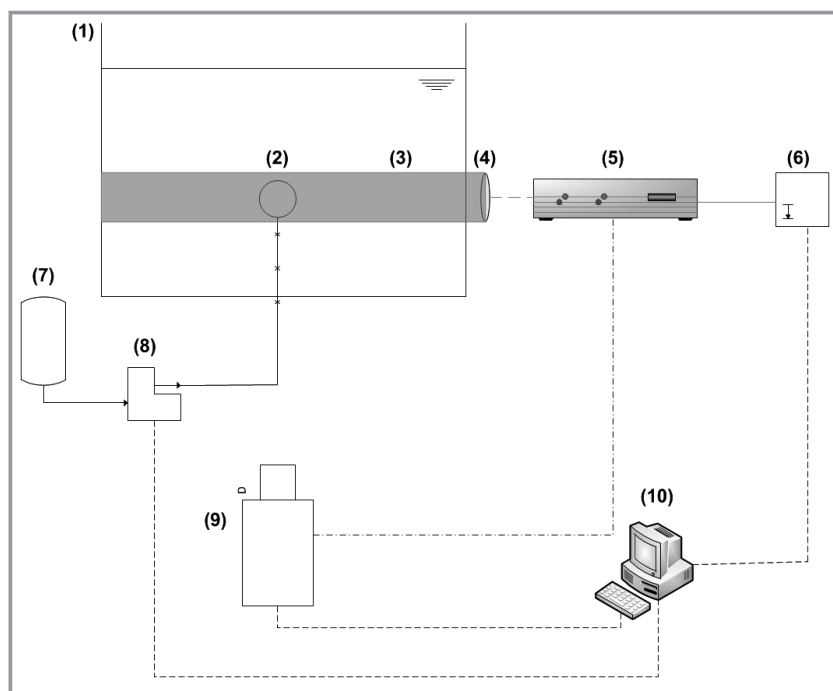


Figure 2. Experimental setup for LIF measurements [6]: (1) measurement cell, (2) droplet at capillary, (3) widened laser beam, (4) optics, (5) laser beam shutter, (6) laser, (7) storage tank, (8) precision syringe pump, (9) high-speed camera, (10) computer.

taken. The calibration for the rhodamine 6G is described in [5]. Interfacial tension measurements have shown no effect for the very low dye concentrations applied here.

2.2 Rainbow Schlieren Deflectometry at TU Berlin

The experimental setup used at TU Berlin for application of rainbow schlieren deflectometry is shown in Fig. 3. The setup is a slightly modified version of the one introduced in Schulz et al. [22] where in combination with Schulz et al. [23] its application for qualitative mass transfer measurements and quantitative heat transfer measurements has been shown successfully. The setup is based on an optical aluminum rail (type X95) as main axis where the optical components are aligned on. An optical cage system is used for precise alignment of the optical components. For positioning of the mass transfer test cell described in Sect. 2.3 the optical cage system is opened between the collimating and the collecting lens. In contrast to [22] the laser-driven broadband light source (LDLS) Energetiq EQ-99XFC is used for illumination and fiber-coupled ($d = 230$ μm, $NA = 0.22$, $L = 1$ m) to a 30 μm wide slit aperture, which is fixed at the center of the optical cage and defines the main optical axis. An iris diaphragm is used to control the diameter of the light beam emitted through the apparatus to reduce optical aberration.

Light emitted through the source aperture acts as point light source and is positioned in the focal point of an achromatic lens (focal length $f_1 = 250$ mm, diameter $d_L = 50.8$ mm) for collimation. A second achromatic lens is used for refocusing the collimated light rays and its focal length is chosen according to the desired magnification and measurement sensitivity. The mass transfer test cell introduced in Sect. 2.3 is positioned between the collimating and the collecting lens. For RSD measurements a color scale filter is positioned in the focal plane of the collecting lens via a yz -translation mount for rectangular optics. Inspired by Greenberg et al. [14] one-dimensional color scale filters with linear change of hue value in one direction and constant hue values in the other direction are applied (see [22] for details and calibration of the system). A colored 4 MP CMOS-highspeed camera (Vieworks VC-4MC-C180EO-CM) is used in conjunction with a 12x Zoom lens (LaVision) for magnification. From the resulting images the hue value of each pixel can be extracted. By comparison with the respective values in the undisturbed reference image and by

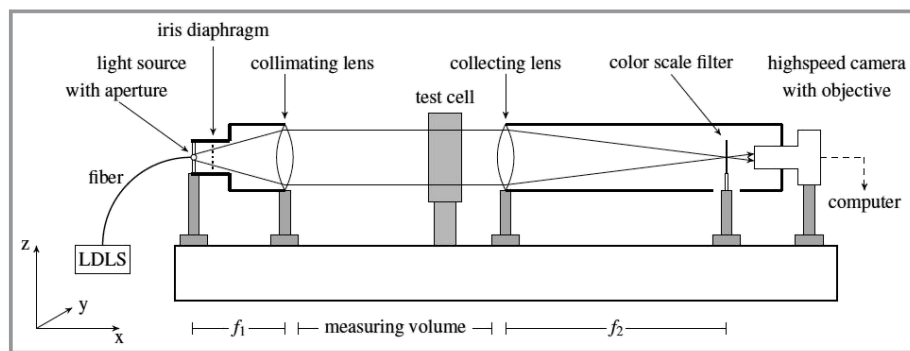


Figure 3. Experimental setup applying RSD (slightly modified from [22]) with mass transfer and coalescence test cell from [24].

application of the calibration curve differences in hue values between the experimental and reference image can be correlated to the displacement on the filter in y or z direction. In case of symmetric distributions, quantitative evaluation of the projected refractive index gradient field would be possible. For asymmetric concentration fields the evaluation is of qualitative nature or multiple viewing angles would be needed [14].

2.3 Mass Transfer Test Cells for Optical and Suction Measurements

The test cells used for the optical measurement of mass transfer at both institutes are well established and have been introduced in Heine and Bart [5] and Villwock et al. [24] respectively. Comparability is ensured by control of the main parameters influencing the mass transfer during droplet production, e. g., disperse to continuous phase ratio, capillary diameter and material and sufficient cleaning procedures.

The suction experiments at TUK are performed in a separate measuring test cell specifically designed for the suction experiments [5], while the mass transfer samples at TU Berlin are collected in the test cell introduced in Wegener et al. [25] for mass transfer measurements during droplet production. Comparability is still ensured since both experimental setups are well established in their field of application and have been shown to yield accurate and reproducible results [5, 25].

2.4 Materials

Two different reference systems were investigated: System 1 is the standard test system for high interfacial tension proposed by the European Federation of Chemical Engineering (EFCE) in Misek et al. [26] toluene(d)/acetone(s)/water(c). The second reference system chosen consists of 1-octanol(d)/water(c) with butyldiglycol as model transfer component.

All measurements were performed with the mass transfer direction dispersed to continuous phase. In case of acetone in toluene rhodamine 6G was added to the solute while sulforhodamine G was used for the visualization in butyldiglycol/1-octanol. Since the system is highly sensitive to impurities, only chemicals of high purity have been used, see Tab. 2 for details. Relevant physical properties of all components are also shown in Tab. 2. Water was purified via reverse osmosis

and additional ion exchanger yielding a conductivity of less than $0.5 \mu\text{S cm}^{-1}$ and total organic carbon below 3 ppm. The binary systems of disperse and continuous phase were mutually saturated to avoid additional mass transfer.

3 Results and Discussion

The droplet formation as well as the pendant drop in the aforementioned reference systems has been investigated by LIF and RSD measurements. Identical parameters were used for comparability to investigate the influence of formation rate, initial solute concentration and droplet size on mass transfer. Each figure is comprised of RSD results to the left and LIF results on the right side and shows exemplarily a sequence of different time steps representing the contact time between the disperse and the continuous phase. The time for drop production depends on the volumetric flow rate in conjunction with the final drop diameter. After dispensing the desired volume, the drop stays attached to the capillary, which represents the phase called “pendant drop”. Tab. 3 summarizes the parameters held constant or varied between the chosen sequences for comparison.

The grey values in the LIF measurements have a linear relationship with the concentration as described in [5] for rhodamine 6G. For the measurements, the initial concentration was set to pure white at the beginning. Thus, at high concentration and low volumetric flow rate the drop appears very dark right after formation, because the mass transfer during droplet formation already leads to a much lower concentration compared to the initial concentration.

3.1 Experimental Results for Toluene/Acetone/Water

A sequence of droplet formation with a final diameter of 2.5 mm is shown in Fig. 4 with a volume flow of $5 \mu\text{L s}^{-1}$ and an initial concentration of 2.5 wt %.

Table 2. Physical properties of applied systems at 25 °C: data for toluene/acetone/water from [26] with interpolation concerning the temperature dependence if needed, diffusion coefficients for butyldiglycol calculated via [27]).

Component	Density ρ [kg m ⁻³]	Viscosity μ [mPa s]	Partition coefficient K [-]	Diffusivity in (c) D_{sc} [m ² s ⁻¹]	Diffusivity in (d) D_{sd} [m ² s ⁻¹]	Purity/Producer
Water (c)	997.2	0.8903				$\kappa < 0.5 \mu\text{S cm}^{-1}$ TOC < 3 ppm
<i>System 1</i>						
Toluene (d)	862.3	0,552				> 99.8 % (Fischer Chemical)
Acetone (s)	784.4	0.304	0.93	1.13×10^{-9}	2.7×10^{-9}	> 99.9 % (BDH® Chemicals)
<i>System 2</i>						
1-Octanol (d)	821.6	7.288 [28]				> 99 % (Honeywell)
Butyldiglycol (s)	948.2	5.232 [29]	3.66	5.96×10^{-10}	1.86×10^{-10}	> 99 % (Sigma Aldrich)

Table 3. Chosen parameter sets included in this publication (system 1: toluene/acetone/water, system 2: 1-octanol/butyldiglycol/water).

System	Fig. no.	Initial solute conc. [wt %]	Final diameter [mm]	Volumetric flow rate [$\mu\text{L s}^{-1}$]	Time for drop formation [s]	Focus on
1	4	2.5	2.5	5	1.64	reference
1	5	2.5	2.5	10	0.82	flow rate
1	6	10	2.5	5	1.64	initial conc.
1	7	10	2.5	10	0.82	flow rate
1	8	5	3.5	10	2.25	final diameter
1	9	5	1.5	5	0.35	final diameter
2	10	8	2.3	8.33	0.77	test system

During droplet formation in the system toluene/acetone/water it can be seen that the solute distribution is inhomogeneous. Fig. 4 shows a higher concentration of solute flowing along the right side of the droplet during the initial stages of drop production (0.35 to 1.23 s), which also leads to higher mass transfer and therefore higher concentration gradients on the right side outside of the drop as visualized by schlieren imaging. Taking a closer look at the top right of the drop small deviations of solute concentration can be observed, which lead to movement of the interface (LIF) and disturbance of the outer concentration boundary layer by Marangoni flows shown by RSD (see, e.g., region indicated at 1.23 s). Thus, a causal relationship of time and place dependence between the concentrations inside the droplet and the schlieren or concentration gradients respectively outside the droplet can be shown. During further formation the high concentration is distributed more uniformly in the droplet by the volumetric flow rate, whereby the mass transfer takes place more evenly around the drop-

let. Due to the initial concentration difference, there are always compensating currents, the Marangoni convection.

However, if the volumetric flow rate is increased, as shown in Fig. 5, a more homogenous concentration in the droplet can be observed during droplet formation. As soon as the droplet formation is finished, Marangoni convection occurs as a result of the concentration differences seen in the first row of Fig. 5 for a contact time of 0.8 s, which is alternated by diffusive time periods, as can be seen at 5.78 s. However, when concentration gradients develop again, Marangoni convection occurs again disturbing the concentration boundary layer by inducing interfacial turbulence which can be observed after more than 10 s of contact time shown in the last row of Fig. 5. Overall, the mass transfer decreases over time, which also reduces Marangoni convection. The eruptions can also be triggered by mass transfer through the opening of the capillary.

In general, interfacial instability (turbulent, eruptive) [10, 11] is prominent at solute mass fractions of 1 wt % and

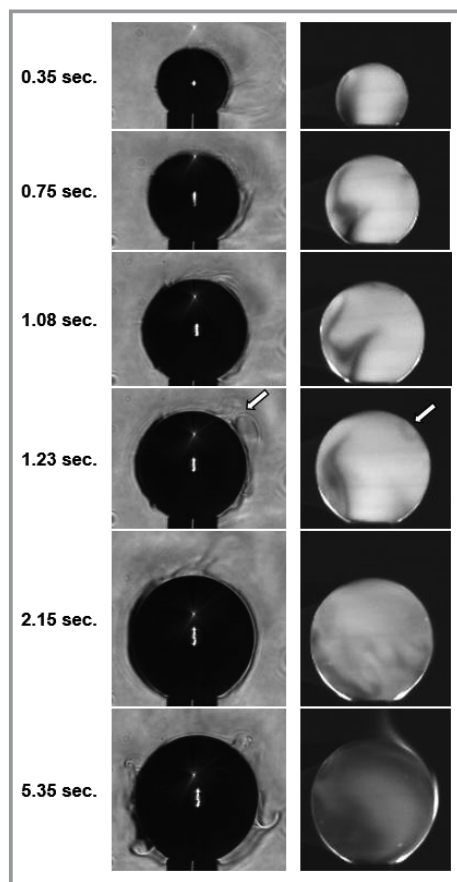


Figure 4. Sequence of droplet formation with a final diameter of 2.5 mm, volumetric flow rate $\dot{V} = 5 \mu\text{L s}^{-1}$ and initial solute concentration of 2.5 wt % in the system toluene/acetone/water, left: RSD images (RSD images were converted to grey-scale for publication purposes. The raw images comprise hue values between 0 and 0.9 in the HSI color scheme.), right: LIF images with $0.005 \text{ mmol L}^{-1}$ of rhodamine 6G.

higher in the system observed here [6]. By increasing the acetone mass fraction to 10 % (Fig. 6), the convective flow is much more pronounced. The characteristic lateral displacement of the drop attached to the capillary by momentum transfer connected to intense mass transfer [6, 25] can be observed. The flow of high acetone concentration is directed to the right at the capillary, causing the phase boundary to move significantly. Since the mass transfer intensification by interfacial tension gradients is much more pronounced, the drop has a significantly lower concentration during and after formation, which was also observed in [3, 4, 30, 31] stating extraction rates up to 60 or even up to 80 % [32] in case of drop formation in the presence of interfacial instabilities.

Higher volumetric flow rates may change this behavior. In Fig. 7 the increased volume flow dominates the mixing in the droplet, thus the concentration in the droplet is distributed and the typical vortices are formed, which also occur in case of rising droplets in a stagnant fluid [33]. Nevertheless, Marangoni convection is clearly visible by RSD, as well

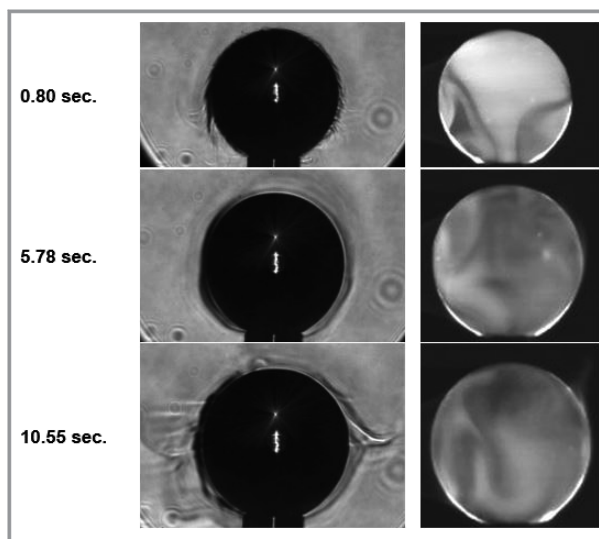


Figure 5. Sequence of droplet formation with a final diameter of 2.5 mm, volumetric flow rate $\dot{V} = 10 \mu\text{L s}^{-1}$ and initial solute concentration of 2.5 wt % in the system toluene/acetone/water, left: RSD images, right: LIF images with $0.005 \text{ mmol L}^{-1}$ of rhodamine 6G.

as the stronger mass transfer on the right side due to convection. After the formation is finished at approximately 0.8 s, the mass transfer on both sides is equally intensified by instabilities and the onset of convection shifts to the upper hemisphere of the drop, disturbed occasionally by eruptive flows alternating between the right and the left side of the drop (see Fig. 7 at 2.1 s and following (right side)).

In Figs. 8 and 9 the influence of the final diameter after drop production is compared. Fig. 8 shows the experimental results for the drop production of a drop with a final diameter of 3.5 mm and an initial solute concentration of 5 wt %. The inner vortices induced by the volumetric flow rate and the curvature of the drop interface can be identified. A flow of high concentration is oriented vertically in the center of the drop. By following the curvature of the drop the flow is redirected, thus creating the inner circulation. As a result, the phase boundary moves downwards too, which can also be seen by the downward movement of the schlieren (0.23–2.28 s). Due to the size of the droplet, the inner vortices stay longer intact after formation (2.7 s), which still affects the development of the outer concentration field as visualized by the schlieren measurements around the droplet. When the vortices further decrease in intensity, the same behavior as described above can be observed. With increased contact time the mass transfer gets less intense and, as described above, convective and diffusive phases (16.35 s) alternate until the mass transfer finally stays diffusive at the end.

However, with a final diameter of 1.5 mm, as shown in Fig. 9, the time and volume to induce vortices inside the droplet by the volumetric flow rate is much shorter compared to Fig. 8. The first row of Fig. 8 with timestamp 0.23 s is identical to Fig. 9, but the formation in case of the 1.5 mm

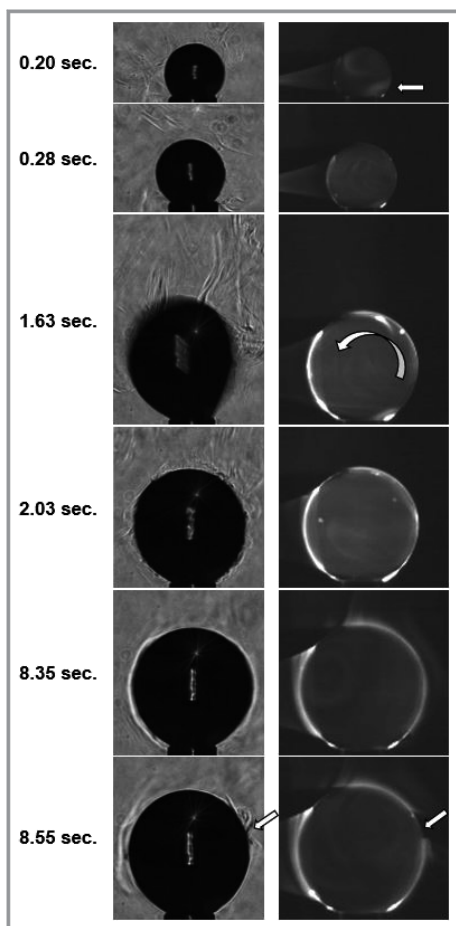


Figure 6. Sequence of droplet formation with a final diameter of 2.5 mm, volumetric flow rate $V = 5 \mu\text{L s}^{-1}$ and initial solute concentration of 10 wt % in the system toluene/acetone/water, left: RSD images, right: LIF images with 0.02 mmol L^{-1} of rhodamine 6G (sharp ridges on the left hand side result from the lens effect of the drop interface)

drop in Fig. 9 is finished at 0.35 s. As can be seen, the vortexes start to get disturbed earlier by the mixing effect of the Marangoni currents for smaller droplets, see the first row of Fig. 9, showing a contact time of 0.4 s. The transition component is distributed differently inside the drop, with the concentration on the left side being significantly lower than on the right side, which is a result of the higher concentration differences on the left side in the beginning leading to a stronger convective flow pattern induced by Marangoni forces shown on the left side of the drop by RSD.

3.2 Experimental Results for 1-Octanol/Butyldiglycol/Water

If the substance system is now changed to 1-octanol(d)/butyldiglycol(s)/water(c), a clearly different behavior can be

observed. The mass transfer is slower compared to the system toluene(d)/acetone(s)/water(c). Marangoni convection can still be observed, but it is less pronounced and the movement of the drop and the outer concentration boundary layer is less intense and shows a lower frequency. Furthermore, in Fig. 10 it can be seen that the convection flow spreads differently in contrast to the previously observed behavior of the system toluene/acetone/water.

The mass transfer starts at the top of the droplet and spreads downwards, thus creating a flow around the droplet which transports the transition component downwards by free convection. Subsequently, the transition component stays in the vicinity of the drop and the Schlieren sediment in direction of the capillary. This behavior can be explained by the change of density of the mixture between the transition component and water as continuous phase (Fig. 11). Due to negative excess volume, the density of the mixture increases above the value of pure water for butyldiglycol mass fractions between 0 and approximately 30 wt %, which explains the slow sedimentation in direction of the gravitational force. With increasing solute concentration the density reaches a maximum of close to 1000 kg m^{-3} . The small deviation in densities leads to much slower movement of the schlieren observed in the continuous phase. At approximately 30 wt % the density decreases below the reference value of pure water.

However, Marangoni convection is also decisive for the increased mass transfer in this system compared to the theoretical value for a fluid particle without interfacial instability. This can be seen by the internal mixing visualized in the droplet via LIF measurement and also by the transient, irregular movement of the concentration boundary layer around the droplet shown by RSD.

As mentioned above, mass transfer in the system 1-octanol/butyldiglycol/water is much slower compared to the system toluene/acetone/water. By visual observation, Marangoni convection could be verified in both systems, though differing in intensity. By means of droplet suction, the qualitative observation can be supported by quantitative data: The droplet was formed and directly sucked off or either attached to the capillary for a certain contact time and then sucked off to be analyzed by gas chromatography. Fig. 12 shows the difference in extraction efficiency ($E = 1 - w \times w_{\text{So}}^{-1}$) for varying contact times for both systems indicating higher mass transfer rates for the system toluene/acetone/water. For one thing, this can be explained by the difference in diffusion coefficients (see Tab. 2) and investigated diameters (see Tab. 3) favoring faster mass transfer in that system.

By comparing the results with reference to the Fourier numbers ($Fo = 4DtR^{-2}$), the influence of diffusion coefficient and diameter can be seen in Fig. 13. Though the extraction efficiency in the system 1-octanol/butyldiglycol/water (\blacktriangle) for the highest contact time or lowest Fourier number respectively and the value for toluene/acetone/water with 5 wt % initial solute concentration (\diamond) for the

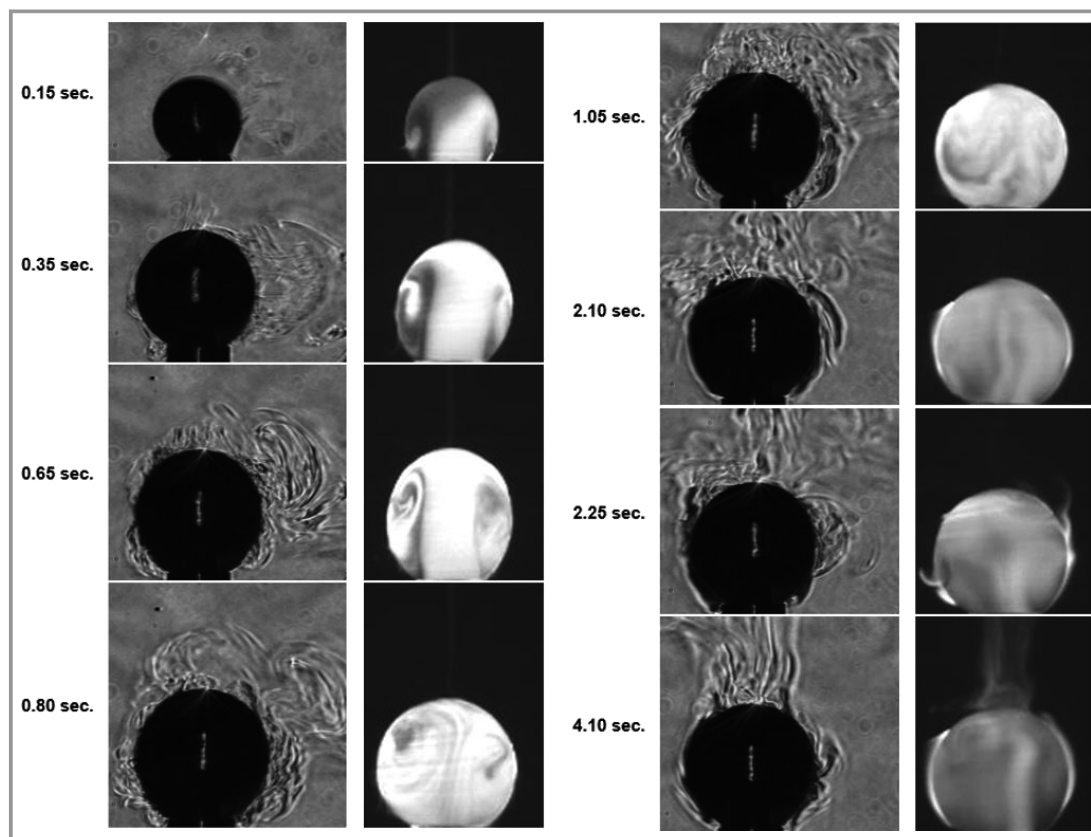


Figure 7. Sequence of droplet formation with a final diameter of 2.5 mm, volumetric flow rate $\dot{V} = 10 \mu\text{L s}^{-1}$ and initial solute concentration of 10 wt % in the system toluene/acetone/water, left: RSD images, right: LIF images with 0.02 mmol L^{-1} of rhodamine 6G.

lowest Fourier number fit together. However, the mass transfer rate is directly connected to the slope of the data points, which is distinctively higher for the toluene/water system and therefore supports the claim of lower mass transfer rates for the 1-octanol/water system. However, this finding is also in combination with the partitioning behavior and the varying initial solute concentrations not sufficient to explain the differences in mass transfer rates. Therefore, since both systems show convective flows (Marangoni convection) due to interfacial tension gradients with differing intensity and flow patterns, the different Marangoni intensity has to be taken into consideration. Based on the suction experiments, mass transfer of the system toluene/acetone/water is 3–5 times faster in relation to the system 1-octanol/butyldiglycol/water in terms of weight percent in the experiments shown here.

4 Conclusions

The influence of the Marangoni effect on mass transfer at single droplets during and after droplet formation was studied with two independent methods: laser-induced fluorescence (LIF) measurements and Rainbow Schlieren

Deflectometry (RSD), to visualize local concentration distributions inside and around the droplet. For determination of the overall concentration of several droplets, the droplets were additionally sucked off and the concentration determined via gas chromatography. In general, a rapid decrease of the solute concentration during droplet formation and the first seconds after formation could be determined. However, the mass transfer is about 3–5 times faster in the system toluene/acetone/water compared to the system 1-octanol/butyldiglycol/water due to a different Marangoni intensity. The mass transfer enhancement by Marangoni convection during droplet formation could be visualized by LIF and RSD measurements for both systems. By combination of both measuring techniques it could be shown how the turbulent mixing by Marangoni convection inside the droplet is connected to the flow patterns around the droplet. The interfacial instability is strongly pronounced during droplet formation at lower volumetric flow rates. This can be explained by higher concentration gradients, which are caused by the larger surface to volume ratio and less inlet flow with the initial solute concentration, which leads to a faster depletion of the concentration and less homogenization inside the drop. However, at higher volumetric flow rates the inlet flow is dominating the concentration distri-

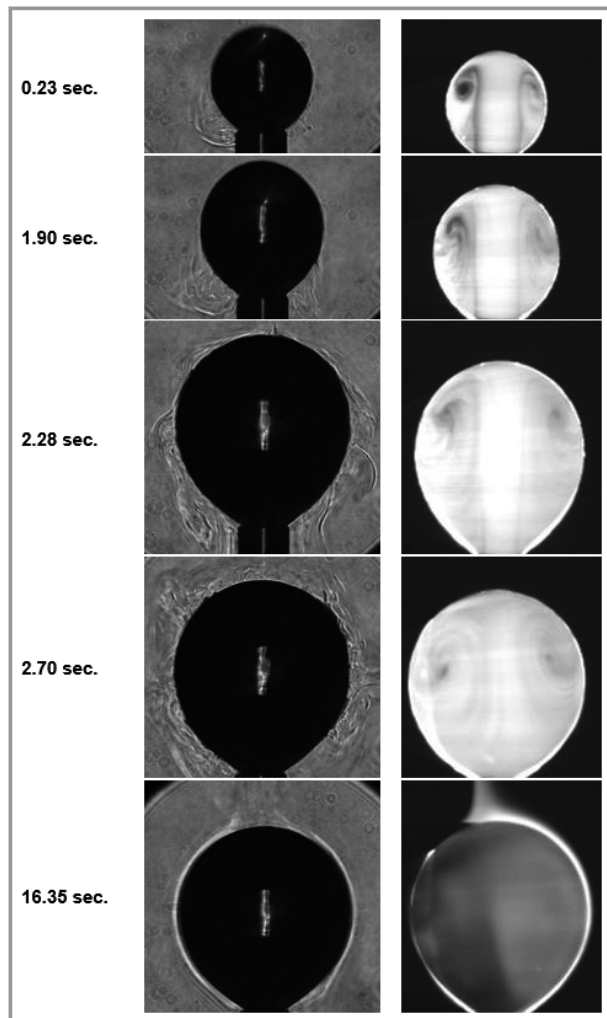


Figure 8. Sequence of droplet formation with a final diameter of 3.5 mm, volumetric flow rate $\dot{V} = 10 \mu\text{L s}^{-1}$ and initial solute concentration of 5 wt % in the system toluene/acetone/water, left: RSD images, right: LIF images with 0.01 mmol L^{-1} of rhodamine 6G.

bution, which reduces the formation of strong concentration gradients as can be seen by LIF and Schlieren measurements in- and outside of the drop. Thus, it can be established that at low volumetric flow rates, the Marangoni convection dominates the mixing inside the droplet and by increasing the volumetric flow rate, the mixing is more dominated by the volumetric flow rate. Furthermore, by comparing the two systems, it could be shown that concentration profiles inside the droplet and thus also around the droplet may differ significantly which is connected to different intensities of the Marangoni effect which is responsible for a different increase in mass transfer rates.

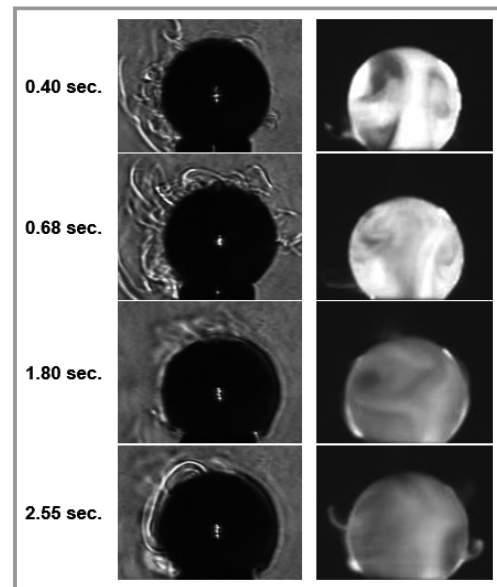


Figure 9. Sequence of droplet formation with a final diameter of 1.5 mm, volumetric flow rate $\dot{V} = 5 \mu\text{L s}^{-1}$ and initial solute concentration of 5 wt % in the system toluene/acetone/water, left: RSD images, right: LIF images with 0.01 mmol L^{-1} of rhodamine 6G.

Financial support by the Deutsche Forschungsgemeinschaft (DFG) is gratefully acknowledged. Gefördert durch die Deutsche Forschungsgemeinschaft (DFG) – TRR 63 "Integrierte chemische Prozesse in flüssigen Mehrphasensystemen" (Teilprojekt A10) – 56091768 und Ba 1569/73-2. Open access funding enabled and organized by Projekt DEAL.

Symbols used

d	[m]	diameter
D	$[\text{m s}^{-1}]$	diffusivity
E	[-]	extraction efficiency
Fo	[-]	Fourier number
R	[m]	radius
t	[s]	time
w	$[\text{kg kg}^{-1}]$	mass fraction
\dot{V}	$[\text{m}^3 \text{s}^{-1}]$	flow rate

Greek symbols

μ	[Pa s]	dynamic viscosity
ρ	$[\text{kg m}^{-3}]$	density
κ	$[\text{S m}^{-1}]$	electrical conductivity

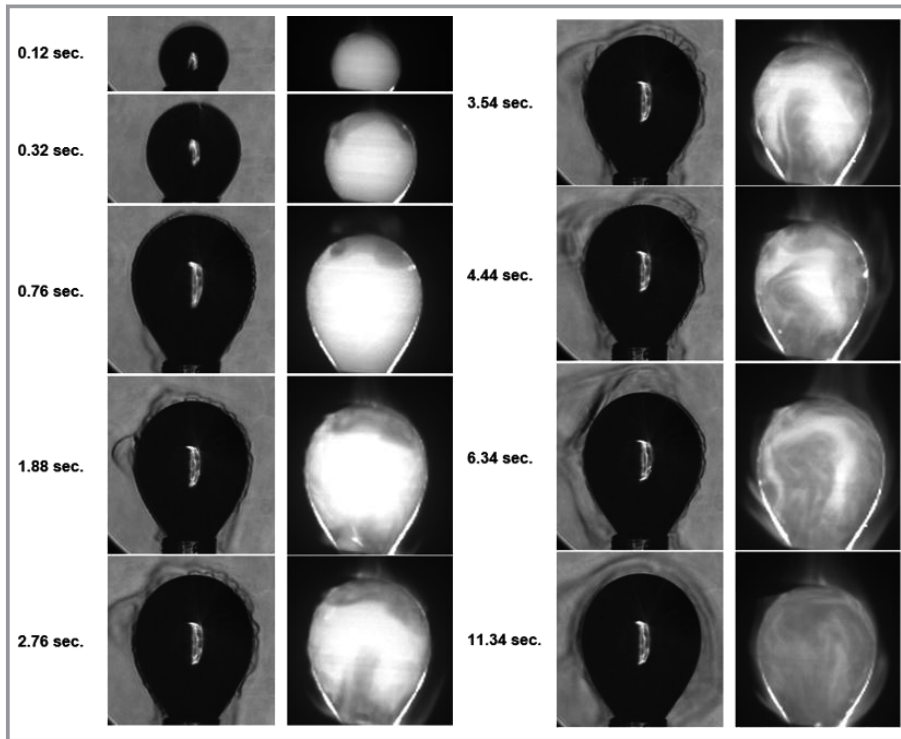


Figure 10. Sequence of droplet formation with a final diameter of 2.3 mm, volumetric flow rate $\dot{V} = 8.33 \mu\text{L s}^{-1}$ and initial solute concentration of 8 wt % in the system 1-octanol/butyldiglycol/water, left: RSD images, right: LIF images with 0.05 mmol L^{-1} of sulforhodamine G.

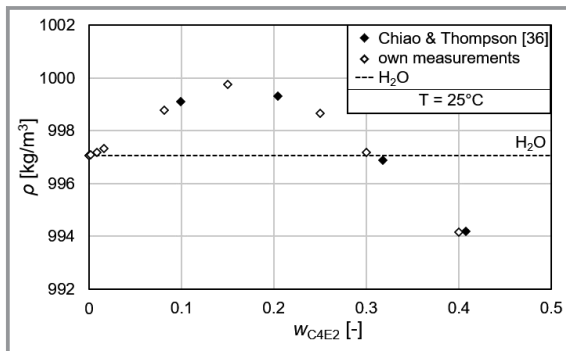


Figure 11. Density of mixtures of 1-octanol with varying butyldiglycol mass fraction at 25 °C.

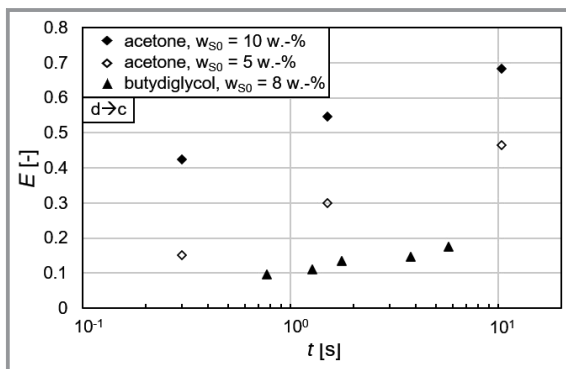


Figure 12. Experimental results for suction experiments for toluene/acetone/water ($d_p = 2 \text{ mm}$, $w_{\text{SO},d} = 5, 10 \text{ wt } \%$, $\dot{V} = 10 \mu\text{L s}^{-1}$) and 1-octanol/butyldiglycol/water ($d_p = 2.3 \text{ mm}$, $w_{\text{SO},d} = 8 \text{ wt } \%$, $\dot{V} = 8.33 \mu\text{L s}^{-1}$) for varying contact times.

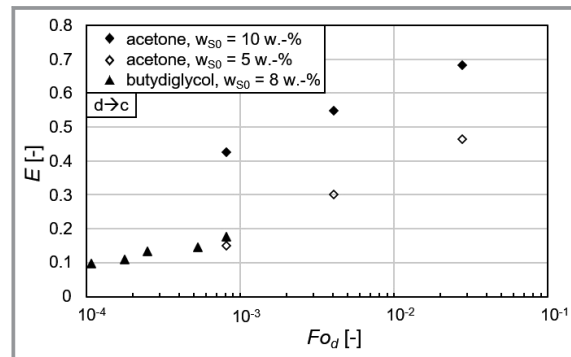


Figure 13. Experimental results for suction experiments for toluene/acetone/water ($d_p = 2 \text{ mm}$, $w_{\text{SO},d} = 5, 10 \text{ wt } \%$, $\dot{V} = 10 \mu\text{L s}^{-1}$) and 1-octanol/butyldiglycol/water ($d_p = 2.3 \text{ mm}$, $w_{\text{SO},d} = 8 \text{ wt } \%$, $\dot{V} = 8.33 \mu\text{L s}^{-1}$) for varying Fourier numbers.

Sub- and superscripts

c	continuous phase
d	disperse phase
p	particle
s	solute
0	initial value

Abbreviations

EFCE	European Federation of Chemical Engineering
fps	frame per second
HSI	hue, saturation, intensity color scheme

LDLS	laser-driven light source
LIF	laser-induced fluorescence
RSD	rainbow schlieren deflectometry
TOC	total organic carbon
TUB	Technische Universität Berlin
TUK	Technische Universität Kaiserslautern

References

- [1] C. Marangoni, *Ann. Phys.* **1871**, 219 (7), 337. DOI: <https://doi.org/10.1002/andp.18712190702>
- [2] F. Gebauer, J. Villwock, M. Kraume, H.-J. Bart, *Chem. Eng. Res. Des.* **2016**, 115, 282.
- [3] W. Licht, J. Conway, *Ind. Eng. Chem.* **1950**, 42 (6), 1151.
- [4] W. Licht, W. Pansing, *Ind. Eng. Chem.* **1953**, 45 (9), 1885.
- [5] J. S. Heine, H.-J. Bart, *Can. J. Chem. Eng.* **2020**, 98, 1164.
- [6] J. S. Heine, H.-J. Bart, *Chem. Eng. Technol.* **2019**, 42, 1388.
- [7] A. Javadi, D. Bastani, M. Taeibi-Rahni, *AIChE J.* **2006**, 52, 895.
- [8] A. Javadi, M. Karbaschi, D. Bastani, J. K. Ferri, V. I. Kovalchuk, N. M. Kovalchuk, K. Javadi, R. Miller, *Colloids Surf. A* **2014**, 441, 846.
- [9] L. Hohl, R. P. Panckow, J. M. Schulz, N. Jurtz, L. Böhm, M. Kraume, *Chem. Ing. Tech.* **2018**, 90 (11), 1709.
- [10] H. Sawistowski, B. R. James, *Chem. Ing. Tech.* **1963**, 35 (3), 175.
- [11] H. Sawistowski, *Chem. Ing. Tech.* **1973**, 45 (18), 1093.
- [12] D. Ambrosini, P. Ferraro, *Opt. Lasers Eng.* **2018**, 104, 1.
- [13] W. L. Howes, *Appl. Opt.* **1984**, 23 (14), 2449.
- [14] P. S. Greenberg, R. B. Klimek, D. R. Buchele, *Appl. Opt.* **1995**, 34 (19), 3810.
- [15] G. S. Settles, *Schlieren and Shadowgraph Techniques – Visualizing Phenomena in Transparent Media*, Springer, Berlin **2001**.
- [16] G. S. Settles, M. J. Hargather, *Meas. Sci. Technol.* **2017**, 28 (4), 1.
- [17] H. Sawistowski, Interfacial Phenomena, in: *Recent Advances in Liquid-Liquid Extraction* (Ed: C. Hanson), Pergamon Press, Oxford **1971**, 293–366.
- [18] D. Agble, M. A. Mendes-Tatsis, *Int. J. Heat Mass Transf.* **2000**, 43 (6), 1025.
- [19] B. Arendt, R. Eggers, *Int. J. Heat Mass Transf.* **2007**, 50 (13–14), 2805.
- [20] Z. Wang, P. Lu, G. Zhang, Y. Yong, C. Yang, Z. S. Mao, *Chem. Eng. Sci.* **2011**, 66 (12), 2883.
- [21] J. S. Heine, H.-J. Bart, *Chem. Ing. Tech.* **2017**, 89 (12), 1635.
- [22] J. M. Schulz, H. Junne, L. Böhm, M. Kraume, *Exp. Therm. Fluid Sci.* **2019**, 110, 109887.
- [23] J. M. Schulz, H. Junne, L. Böhm, M. Kraume, in *Pro. of the 5th Int. Conf. on Experimental Fluid Mechanics*, Universität der Bundeswehr München, Munich **2018**, 226.
- [24] J. Villwock, F. Gebauer, J. Kamp, H.-J. Bart, M. Kraume, *Chem. Eng. Technol.* **2014**, 37 (7), 1103.
- [25] M. Wegener, R. R. Paschedag, M. Kraume, *Int. J. Heat Mass Transf.* **2009**, 52, 2673.
- [26] T. Misek, R. Berger, J. Schröter, *Standard Test Systems for Liquid Extraction*, 2nd ed., EFCE Publications Series, Vol.46, Institution of Chemical Engineers, Rugby, UK **1985**.
- [27] K. Nakanishi, *Ind. Eng. Chem. Fundam.* **1978**, 17 (4), 253.
- [28] *CRC Handbook of Chemistry and Physics*, 95th Ed.tion (Ed: W. M. Haynes), CRC Press, Hoboken, **2014**.
- [29] C. Pal, A. Kumar, *Fl. Phase Eq.* **1998**, 143 (1–2), 241.
- [30] T.-B. Liang, M. J. Slater, *Chem. Eng. Sci.* **1990**, 45, 97.
- [31] F. B. West, P. A. Robinson, A. C. Morgenthaler JR., T. R. Beck, D. K. McGregor, *Ind. Eng. Chem.* **1951**, 43, 234.
- [32] L. Steiner, G. Oezdemir, S. Hartland, *Ind. Eng. Chem. Res.* **1990**, 29, 1313.
- [33] R. F. Engberg, M. Wegener, E. Y. Kenig, *Chem. Eng. Sci.* **2014**, 117, 114.
- [34] T.-T. Chiao, R. Thompson, *J. Chem. Eng. Data* **1961**, 6 (2), 192.